Revised alkenone δ^{13}C based CO₂ estimates during the Plio-Pleistocene

Osamu Seki[1*] and James Bendle[2]

[1]Institute of Low Temperature Science, Hokkaido University, N19W8, Kita-ku, Sapporo, Hokkaido, 060-0819, Japan
[2]School of Geography, Earth and Environmental Sciences, University of Birmingham, Edgbaston, Birmingham, B15 2TT, UK

Correspondence to: Osamu Seki (seki@lowtem.hokudai.ac.jp)

Abstract. Here we revisit reported alkenone δ^{13}C ($\delta^{13}C_{C37}$) based CO₂ records during the Plio-Pleistocene and apply a refined approach to better constrain the dynamic range of CO₂ during the time. Specifically, we consider ways to correct for regional differences in physical oceanographic factors. As a result of our relatively simple approach we find that offsets of ~150 ppm between reported $\delta^{13}C_{C37}$ CO₂ records from different sites can be significantly reduced. This confirms that better constraints on environmental variables, including physical oceanographic controls on depth and season of production are key aspects for improving $\delta^{13}C_{C37}$ based CO₂ estimates. The revised $\delta^{13}C_{C37}$ CO₂ datasets suggest that Plio-Pleistocene CO₂ levels are 180-350 ppm, which is consistent with the most of reported CO₂ reconstructions, though their upper end of Pliocene CO₂ levels are lower than that of some CO₂ estimates.

1 Introduction

The reconstruction of CO₂ levels in the past is a crucial objective in palaeoclimate research. Continuous, reliable CO₂ records in the past have come from direct measurements of CO₂ in ice-cores (Siegenthaler et al., 2005; Lüthi et al., 2008). However, the currently available (continuous) ice-core based CO₂ record is limited to the past 800 kyrs (Lüthi et al., 2008). To reconstruct the continuous CO₂ record in the past, through warmer climatic base-lines (which predate the ice core record), indirect methodologies such as proxies and models must be applied. Several proxies have been proposed and applied to reconstruct CO₂ in the geologically deep past (Beerling and Royer, 2011). Reconstructed CO₂ data significantly contribute to constraining climate evolution and linkages to the carbon cycle. For instance, recent CO₂ reconstructions in the Cenozoic era indicate that a long-term decline in CO₂ levels was a key driver of global cooling and major glaciations in the Cenozoic (Kürschner et al., 2008; Hönisch et al., 2009; Pearson et al., 2009; Pagani et al., 2011; Beerling and Royer, 2011; Zhang et al., 2013; Greenop et al., 2014; Anagnostou et al., 2016; Cui et al., 2020; Anagnostou et al., 2020; Raitzsch et al., 2021).

The climate evolution from the Pliocene to the Pleistocene, characterized by a transition from warmer than the present climate to the Pleistocene cold-house, is one of the most dramatic climatic changes of the late Neogene. In order to better understand the role of CO₂ in Plio-Pleistocene climate evolution, CO₂ reconstruction has been conducted based on geochemical and botanical approaches including phytoplankton δ^{13}C (Pagani et al., 2010; Seki et al., 2010; Badger et al., 2013; Stoll et al., 2019;

30 Badger e t al., 2019), carbonate $\delta^{11}B$ (Bartoli et al., 2011; Martínez-Botí et al., 2015; Chalk et al., 2017; Dyez et al., 2018; de la Vega et al., 2020), paleosol (Da et al., 2019), terrestrial plant $\delta^{13}C$ (Cui et al., 2020) and leaf stomata (Kürschner et al., 1996). The most widely applied in recent decades derive from analyses of $\delta^{13}C_{C37}$ (Pagani et al., 2010; Seki et al., 2010; Badger et al., 2013; Badger et al., 2019) and planktic foraminiferal $\delta^{11}B$ (Bartoli et al., 2011; Martínez-Botí et al., 2015; Dyez et al., 2018; de la Vega et al., 2020) in marine sediment cores recovered from the different parts of the global ocean (Fig. 1).

35 The accumulated data from this research effort suggests that CO_2 played a substantial role in Plio-Pleistocene climate evolution (Fig. 2b). However, although all the proxy CO_2 records show the long-term decreasing trend throughout the Plio-Pleistocene, absolute estimates of CO_2 level markedly differ among the data, ranging from 200 to 600 ppm (Fig. 2b). The wider range of CO_2 estimates may be attributed to variable $\delta^{13}C_{C37}$ CO_2 estimates depending on distinct oceanographic settings (Seki et al., 2010; Pagani et al., 2005) and large offset of $\delta^{11}B$ estimates between the different foraminifera species (Martínez-Botí et al.,

40 2015; Dyez et al., 2018). Of course, fundamental advances and refinements in our understanding of the $\delta^{13}C_{C37}$ proxy, beyond the model conceptualized by Pagani et al. (2002) are possible, and progress is being made in this regard. For example in a) constraining the influence of growth rate (μ), cell size (r), and membrane permeability (P) on the empirical 'b' factor (Bolton et al., 2015; Stoll et al., 2019; Zhang et al., 2020) and b) on emerging culture-based models, which will attempt to quantitatively consider the influence of cell size and irradiance (Phelps et al ., 2020). However, here we use the original "Pagani" et al. (2002)

45 diffusive transport model which built on earlier work by Bidigare et al. (1997, 1999). Our aim is not to provide newly definitive CO_2 estimates but to demonstrate the importance of physical oceanography, as all $\delta^{13}C_{C37}$ CO_2 reconstructions (even using refined models) rely on some assumptions that are sensitive to regional oceanographic settings (Pagani et al., 2011). Not correcting for these differences can yield errors up to 150 ppm for individual sites and regions (Pagani et al., 2010). This is demonstrated by the relatively higher alkenone based $\delta^{13}C_{C37}$ CO_2 values (>350 ppm) in the Pleistocene (Pagani et al., 1010),

50 which are inconsistent with blue ice derived CO_2 data which show that the late Pliocene CO_2 levels do not exceed 280 ppm (Voosen, 2017; Yan et al., 2019).

$\delta^{11}B$ CO_2 (Foster et al, 2008; Chalk et al., 2017) seems to represent better the late Pleistocene glacial-interglacial CO_2 fluctuations observed in ice-core CO_2 records (Siegenthaler et al., 2005), and thus likely provide more reliable estimates than alkenone $\delta^{13}C_{C37}$ CO_2 (Pagani et al., 2010; Seki et al., 2010; Badger et al., 2013). However, a recent study has exhibited

55 Pliocene CO_2 estimates markedly differ among planktic foraminiferal species (*Globigerinoides ruber* (*G. ruber*) vs. *Torilobatus sacculifer* (*T. sacculifer*)) (Dyez et al., 2018). Subsequently, an attempt was made to reconstruct CO_2 based on the $\delta^{13}C_{C37}$ method with a statistical model approach that constrained the physiological factors and the active carbon transport mechanism, which affects CO_2 reconstruction (Stoll et al., 2019). The attempt resulted in a much wider range of CO_2 in the Pliocene (200-620 ppm). Thus, there is still room for verification in terms of an absolute values and dynamic ranges of CO_2

60 (Fig. 2b). Here, we revisit globally distributed $\delta^{13}C_{C37}$ CO_2 estimates from the Pliocene to today, refine the methods (within the framework of the original Pagani model), and then attempt to reconcile the discrepancies in the published $\delta^{13}C_{C37}$ CO_2 records that span the last 5 Myrs.

2 Material and Methods

2.1 Sample information and chronology

65 Locations of ODP sediment cores used in this study are shown in Fig. 1. We utilize and reinterpret previously published Plio-Pleistocene CO_2 datasets (Sites 806, 925, 982, 999, 1208, and 1241) from Pagani et al. (2010) and Seki et al. (2010). Table 1 provides sample information for the data compiled in this manuscript. Information used in revising CO_2 estimates are shown, including the surface mixed layer (SML) depth and phosphate concentrations ($[PO_4^{3-}]$) derived from the WOA09 (Locarnini et al., 2009), the air-sea CO_2 disequilibrium from Takahashi et al. (2009), the regressions applied to calculate the 70 physiologically dependent b-term, and sea surface temperature (SST).

2.2 $\delta^{13}C_{C37}$ CO_2 proxy based on the diffusive transport model

The $\delta^{13}C$ values of alkenones produced by haptophyte algae, combined with foraminiferal records of surface ocean dissolved inorganic carbon $\delta^{13}C$, can be used to calculate haptophyte carbon isotopic fractionation of (ε_p) during photosynthesis. This, in turn, is related to the concentration of aqueous CO_2 in ocean surface waters (Pagani et al., 2002; Bidigare et al., 1997, 1999). 75 In areas of air-sea equilibrium and where paleo-SST can be determined from $U_{37}^{K'}$ paleothermometry, $[CO_{2(aq)}]$ can be used to determine CO_2.

2.3 Calculation of mixed layer temperatures

For all previously published data, temperatures in the surface mixed layer were estimated from $U_{37}^{K'}$ paleothermometry. In this study, $U_{37}^{K'}$ indices in sediments were converted into growth temperatures using the equation of Sonzogni et al. (1997) that is 80 optimized to high SSTs >24 ºC for Sites 806, 925, 999, and 1241, whereas the global core top derived calibration of Conte et al. (2006) was applied to the extratropical sites (Sites 982 and 1208). The analytical precision of $U_{37}^{K'}$-derived temperature from replicate analyses is ±0.3 ºC.

2.4 Calculation of $\varepsilon_{p37:2}$ values

The carbon isotope fractionation by haptophyte algae during photosynthesis ($\varepsilon_{p37:2}$), is calculated from the $\delta^{13}C$ values of di-85 unsaturated alkenone and the calcite shells of planktic foraminifera using the following equation:

$$\varepsilon_{p37:2} = \left[\frac{(\delta CO_{2(aq)} + 1000)}{(\delta org + 1000)} - 1 \right] \text{ x } 1000 \tag{1}$$

where $\delta CO_{2(aq)}$ and δorg are the $\delta^{13}C$ values of $CO_{2(aq)}$ and haptophyte biomass, respectively. The former is determined from the carbon isotopic composition of *T. sacculifer* and *G. ruber*, as well as the temperature-dependent relationship between $\delta CO_{2(aq)}$ and $\delta CaCO_3$ (Romanek et al., 1992; Mook et al., 1974). SSTs were estimated from the $U_{37}^{K'}$ paleotemperature proxies

90 as discussed above. δorg is derived from the $\delta^{13}C$ values of di-unsaturated alkenones and corrected for the 4.2‰ depletion of alkenones relative to biomass (Bidigare et al., 1997).

2.5 Calculation of CO₂

The ε_p values of marine algae are a function of not only $CO_{2(aq)}$ but also growth rate (Bidgare et al., 1997) and cell geometry (Popp et al., 1998). Therefore, correction of those effects on ε_p values is required. Field and experimental work both indicate

95 that the relationship between ε_p and related factors is expressed as the following:

$$\varepsilon_p = \varepsilon_p - \frac{b}{\{CO_{2(aq)}\}} \tag{2}$$

where ε_f is the isotope fractionation associated with carbon fixation by the ribulose-1,5-bisphosphate carboxylase/oxygenase (RuBisCO) enzyme (25 ‰; Bidigare et al., 1997). The b-term is an expression of physiological factors – including growth rate, membrane permeability, and cell geometry – that affect carbon discrimination by regulating the flux of CO_2 into and out of

100 the cell. For $\delta^{13}C_{C37}$-derived ε_p values, and thus for the limited range of organisms synthesizing such compounds and for which cell geometry effects are thought to be minimal, field data reveal a significant correlation between the b-term and $[PO_4^{3-}]$ (Bidigare et al., 1997; Pagani et al., 2005) (Fig. 3):

$$b = 118.52x[PO_4^{3-}] + 84.07 \; (r^2 = 0.78) \tag{3}$$

The modern range of $[PO_4^{3-}]$ in the surface mixed layer is used to calculate b-term. Because a reliable $[PO_4^{3-}]$ proxy is not

105 available so far, we assume that $[PO_4^{3-}]$ did not differ for the open marine settings in Fig.1 over the last 5 Myr. Finally, atmospheric CO_2 levels are calculated using these b-term values and assuming air-sea equilibrium (using salinity, SSTs, and Henry's Law to convert $CO_{2(aq)}$ to gas CO_2; Weiss, 1974).

3 Result and discussion

3.1 $\delta^{13}C_{C37}$ derived CO_2 records based on the standard diffusive model approach

110 Figure 4a shows CO_2 records derived from the standard approach used in most previous publications: We have calculated the b-term using the global regression (Pagani et al., 2005), which assumes alkenone production depths at the surface of the mixed layer, and which assumes air-sea equilibrium at all sites. Although the trends are generally similar, indicating decreasing CO_2 levels over the past 5 Myr, the ranges are large (>150 ppm) in both recent and older sediments. In particular, CO_2 estimates are relatively low in the extra-tropics (Sites 982 and 1208) and higher in the tropics (Sites 806, 925, and 1241) except for the

115 Caribbean Sea (Site 999).

The first application of the alkenone $\delta^{13}C_{C37}$ CO_2 proxy suggested it could be used to accurately reconstruct $[CO_{2(aq)}]$ when SSTs and the b-term are well constrained (Pagani et al., 2002). If constraints on those parameters are the key to reconstruct

CO$_2$ from the proxy, the observed large gaps among the sites could be attributed to insufficient constraints on such key parameters. It should be noted that the ε_p value of marine algae is a function of not only [CO$_{2(aq)}$], but also the b-term. Modern ranges of [PO$_4^{3-}$] in the euphotic zone are typically used to determine the b-term in paleo-investigations (Seki et al., 2010; Pagani et al., 2010). However, the relationship between the b-term and [PO$_4^{3-}$] depends on the oceanographic setting, resulting in significant variability in the global regression equation (Bidigare et al., 1997; Pagani et al., 2005) (Fig. 2). Therefore, we applied regional rather than global regressions to better constrain the b-term at specific sites (Site 806 and 1241; Fig. 4c; see *Section 3.2.* for the detail). Another factor in CO$_2$ determination is regional variation in air-sea disequilibrium (ΔCO$_2$). Previous studies have reconstructed CO$_2$ levels based on the assumption of equilibrium between CO$_2$ in seawater and the atmosphere. However, air-sea ΔCO$_2$ spatially varies, generally with excess [CO$_{2(aq)}$] in the tropics and deficiencies in the extratropics (Takahashi et al., 2009). Hence, we have reconsidered these data by first correcting for disequilibrium between ocean and atmosphere (Fig. 4b; See *Section 3.3.* for details). Also, we discuss other factors that potentially influence CO$_2$ reconstruction in *Sections 3.4. and 3.5.*

3.2 Geographical and temporal variations in the b-term

As suggested by the empirical relationship between the b-term and [PO$_4^{3-}$] in modern surface ocean waters (Bidigare et al., 1997), the growth rate is a primary factor controlling the b-term in diverse phytoplankton, including haptophytes (Bidigare et al., 1997, 1999; Popp et al., 1999). Although that is factored into our calibration at each site, significant past changes in growth rate (which we infer to be broadly correlated to a regime's primary productivity history) will bias CO$_2$ trends and estimates (Mix et al., 2003). For these reasons, we have precluded Sites 882 and 1012, for which there is evidence for strong past oceanographic and productivity variations which are hard to constrain (Pagani et al., 2010).

All of the remaining CO$_2$ data used in this study exhibit similar long-term decreasing trends (Fig. 4a), suggesting that growth rate variations are subordinate controls on long-term trends. However, there are likely local variations in the controls on the b-term. Although there is a strong positive relationship ($r^2 = 0.78$) between phosphate concentration and the b-term in the global dataset (Bidigare et al., 1997, 1999; Pagani et al., 2005), there are systematic variations in the relationship among different oceanographic regimes. For example, b-term values are lower than the global regression trend in the Equatorial Pacific, Southern Ocean, and sub-Antarctic and higher in Santa Monica, the Northeast Pacific, and the Peru upwelling margin (Fig. 3). Such regional differences are not surprising because phosphate is unlikely to limit directly haptophyte growth, which is instead is probably governed by micronutrients (such as iron, zinc, and cobalt) (Bidigare et al., 1997). The relationships between concentrations of phosphate and the actual growth-limiting micronutrients might differ among regions.

Thus, we explore here the application of regional regressions to better constrain the b-term. Currently, regional regressions are available for Sites 806 and 1241 (Equatorial Pacific regression) (Bidigare et al., 1997).

$$b = 109.8 \times [\text{PO}_4^{3-}] + 65.6 \ (r^2 = 0.74) \tag{4}$$

We apply the regional regression (4) to these sites (Table 1).

3.3 Geographical and temporal variations in air-sea disequilibrium

150

As described earlier, the conversion from $[CO_{2(aq)}]$ to atmospheric $[CO_2]$ is based on Henry's Law (Weiss, 1974) and using SSS (Table 1) and SST (described above), while assuming air-sea equilibrium. However, this assumption is likely invalid in some of the settings investigated. There is excess $CO_{2(aq)}$ in the equatorial ocean due to active upwelling and deficiency of $CO_{2(aq)}$ in extratropical regions (Takahashi et al., 2009). Therefore, we also show CO_2 reconstructions, in which we have

155 corrected for air-sea ΔCO_2 at each site (Fig. 4b; correction shown in Table 1).

3.4 Temporal variations in cell geometry

Previous studies showed that variations in haptophyte cell geometry, if significant enough, can potentially affect ε_p values (Henderiks et al., 2007; Bolton et al., 2015; Stoll et al., 2019; Zhang et al., 2020). In a previous study (Seki et al., 2010), we explored the potential effects of such changes based on the approach of Henderiks et al. (2007), who proposed a geometry-

160 corrected b-term using the coccolith size record of *Reticulofenestra*, the postulated alkenone-producing haptophytes in the Caribbean Sea prior to the Pliocene (Kameo and Bralower, 2000). However, applying this approach to Site 999 results in significantly lower CO_2 levels (<150 ppm) for the Pliocene and Pleistocene compared to the other CO_2 estimates (Kürschner et al., 1996; Siegenthaler et al., 2005; Badger et al., 2013; Pagani et al., 2010; Martínez-Botí et al., 2015; Cui et al., 2020; de la Vega et al., 2020). This underestimation potentially illustrates the limitations for applying the relationship between

165 *Reticulofenestra* coccolith and cell sizes obtained from early Miocene species to the smaller species of the Pliocene.
Moreover, it has been suggested that *Cyclicargolithus* was the most important alkenone producer during the Miocene (Plancq et al., 2012). Similarly, the alkenone concentration record in Caribbean Sea sediments (Seki et al., 2010) does not resemble that of *Reticulofenestra* abundances (Sites 998, 999, and 1000) (Kameo and Sato, 2000). This decoupling suggests that *Reticulofenestra* may not be a major alkenone producer. Thus, we suggest that a cell geometry correction based on

170 *Reticulofenestrais* is not appropriate for the Caribbean Sea. Therefore, the effect of changes in growth rate and cell geometry of alkenone producers remains uncertain for CO_2 reconstruction. However, the effect of geometry change on b-term is probably not significant on Plio-Pleistocene timescales, since cell size does not significantly change in the tropical ocean during the Plio-Pleistocene (Bolton et al., 2015; Badger et al., 2019).

3.5 Other factors affecting $\varepsilon_{p37:2}$

175 As outlined above, $[CO_{2(aq)}]$ estimates are highly sensitive to the b-term, which represents an integration of various physiological variables but is especially dependent on haptophyte growth rate (Bidigare et al., 1997). Equation (2) implicitly assumes that CO_2 diffuses into the haptophyte cell, even though there is much evidence that haptophytes, including those that produce alkenones, employ carbon concentrating mechanisms (CCMs) (Raven et al., 2011; Reinfelder, 2011). Nor does the model account for the competing requirements for dissolved inorganic carbon for both cell growth and coccolith production

180 and the resultant internal partitioning of the DIC pool. These factors are implicitly considered because Equation (2), as well as

the relationships between the b-term and nutrient concentrations, are empirical (Bidigare et al., 1997). However, the recently developed ACTI-CO model of Bolton and Stoll (2013) reveals the complexity of the controls on haptophyte ε_p values; in particular, it illustrates how isotopic partitioning between organic and inorganic components will be governed by a complex range of environmental and physiological factors. As such, we consider our CO_2 estimates to be semi-quantitative and include

185   them primarily to allow comparison to previous investigations. Nonetheless, the ACTI-CO model still indicates that higher $[CO_{2(aq)}]$ will yield higher ε_p values; as such, we consider the trends in atmospheric CO_2 levels generated from $\delta^{13}C_{C37}$-derived ε_p values to be robust.

3.6 Revised $\delta^{13}C_{C37}$ CO_2 over the past 5 Myrs

With taking the factors described above into account, we revised published CO_2 data from the Pacific Ocean and the Atlantic

190   Ocean. Figure 4d shows revised CO_2 records based on the refined approach (e.g. correcting offsets estimated for both ΔCO_2 and regional $[PO_4^{3-}]$). The large difference (>150 ppm) in CO_2 estimates among sites based on the standard approach (Fig. 4a) has been markedly reduced by ~100 ppm when we apply this refined method (Fig. 4d). Indeed, a combination of corrections, using both regional b-term regressions and accounting for air-sea ΔCO_2, yields similar Pliocene to Pleistocene CO_2 records (Fig. 4d). Importantly, the late Pleistocene CO_2 estimates fall within the range of ice core CO_2 records (Siegenthaler et al.,

195   2005; Lüthi et al., 2008), blue ice CO_2 (Higgins et al., 2015; Voosen, 2017; Yan et al., 2019) and T-inverse model derived CO_2 (van de Wal et al., 2011) except for the glacial periods (for detail in *Section 3.7.*) and ODP 982 (Figs. 4d). Overestimation of CO_2 in ODP 982 suggests that the global regression for calculation of b-term is not suitable to the site.

Despite the importance of oceanographic conditions – export production depth of alkenones, $[PO_4^{3-}]$ depth profiles and their relationship to b-term, air-sea ΔCO_2 – we have assumed that they did not differ markedly in the past. If these parameters have

200   changed significantly over time, this would impact absolute reconstructions of CO_2 levels as well as the temporal trends. As records from several sites all exhibit similar long-term trends, despite representing diverse oceanographic settings, we suggest that these parameters have been relatively stable, or at least a relatively minor factor, over the past 5 Myrs for the open ocean environment. Indeed, a relatively stable b-term on Plio-Pleistocene timescales has been suggested in some regions (Bolton et al., 2015; Mejia et al., 2017; Stoll et al., 2019).

205   ### 3.7 Comparison of $\delta^{13}C_{C37}$ CO_2 records with those derived from the ice cores and other CO_2 proxies

Comparison of ice core and $\delta^{13}C_{C37}$ CO_2 shows that some $\delta^{13}C_{C37}$ CO_2 records based on the global b-term regression are higher than ice core CO_2 data (Fig. 4a). However, the offset is significantly reduced if regional b-term regressions and air-sea ΔCO_2 are applied (Fig. 4d) although $\delta^{13}C_{C37}$ CO_2 estimates are still significantly higher than that of ice core records during the glacial periods. Downward revision of the $\delta^{13}C_{C37}$ based CO_2 estimates in the Pleistocene are consistent well with recent CO_2 estimates

210   based on paleosol, which show low CO_2 values (below 300 ppm) throughout the Pleistocene (Da et al., 2019) (Fig. 2b). The large offsets during the glacial periods are possibly attributed to dramatic changes in growth rates of haptophytes (Benthien et

al., 2005; Zhang et al., 2019), air-sea ΔCO_2 (Jasper et al., 1994) during the pronounced glacial-interglacial cycles in the late Pleistocene or upregulation of algal CCM in the low CO_2 glacial period (Stoll et al., 2019: Badger et al., 2019). Further consideration of reported $\delta^{13}C_{C37}$ CO_2 records in the late Pleistocene reveals that the relationship between $\delta^{13}C_{C37}$ and ice core

215 CO_2 breaks down when dissolved CO_2 concentration falls below 7 μmol/L (Badger, 2021).

It remains unclear how these factors will affect CO_2 estimates in the Pliocene (5.4-2.4 Ma) (see below), and therefore I compare our CO_2 estimates to those recently obtained using the *G. ruber* and *T. sacculifer* $\delta^{11}B$ values of planktonic foraminifera (Seki et al., 2010; Martínez-Botí et al., 2015; Bartoli et al., 2011; Dyez et al., 2018; de la Vega et al., 2020). The revised $\delta^{13}C_{C37}$ CO_2 data suggest relatively low CO_2 levels in the warm Pliocene (250-340 ppm from 3-4.5 Ma). This suggests that CO_2 decreased

220 from the Pliocene to the Pleistocene. Our results agree well with *T. sacculifer* $\delta^{11}B$ CO_2 (230-330 ppm) (Bartoli et al., 2011; Dyez et al., 2018) rather than the *G. ruber* $\delta^{11}B$ CO_2 reconstructions (Seki et al., 2010; Martínez-Botí et al., 2015; de la Vega et al., 2020), which exhibit relatively higher CO_2 levels (250-470 ppm) (Fig. 2b).

The relatively higher *G. ruber* $\delta^{11}B$ CO_2 estimates in the Pliocene could largely reflect an inherently greater CO_2 variability than that recorded by alkenones (Badger et al., 2013). This might be due to the aforementioned impact of important factors not

225 explicitly considered in the Bidigare et al. (1997) model, i.e. CCMs (Stoll et al., 2019) and G-IG variabilities of growth rate (Zhang et al., 2019), cell size, and membrane permeability (Zhang et al., 2020). Zhang et al. (2019) and (2020) argued that term b value substantially varies associated with G-IG cycles in some regions. Discounting this results in an underestimation of $\delta^{13}C_{C37}$ CO_2 variability over the glacial cycles while Badger et al. (2019) suggest the importance of CCMs effect for overestimation of $\delta^{13}C_{C37}$ CO_2 in the glacial low CO_2 conditions. However, CCM unlikely explains relatively low CO_2

230 estimates in the Pliocene since upregulation of CCM results in overestimation of pCO_2 when dissolved CO_2 level is lower than 7 μM (Badger, 2021). Also, it should be noted that the CCM effect is unlikely upregulated in mid to high latitude oceans where the surface water temperature is enough cold and thus dissolved CO_2 concentration in the surface mixed layer is enough high to allow algae to adopt diffusive carbon transport.

Another potential reason for the overestimation of glacial CO_2 is an underestimation of G-IG variability of dissolved CO_2 $\delta^{13}C$.

235 $\delta^{13}C$ of dissolved CO_2 in the past is estimated from $\delta^{13}C$ of foraminifera carbonate shells, which is used to calculate ε_p. A previous study shows that carbon isotope fractionates into foraminiferal calcite as a function of seawater pH/CO_3^{-2} (Spero et al., 19997) which must vary associated with the late Pleistocene G-IG cycle given that ~100 ppm variation of CO_2 as suggested by the ice core CO_2 record. Not considering this effect results in an overestimation of glacial CO_2 levels. However, according to the relationship between foraminiferal $\delta^{13}C$ and CO_3^{-2} (Spero et al., 1997), this effect only explains approximately 10 ppm

240 overestimation during the glacial. Thus, this effect is not sufficient to explain the mute signal of G-IG $\delta^{13}C_{C37}$ CO_2 variability. Stoll et al. (2019) revisited $\delta^{13}C_{C37}$ CO_2 records in the two tropical sites (ODP 925 and 999) and revised estimates based on a statistical multilinear regression model, which accounts for light, growth rate, and [$CO_{2(aq)}$] (Fig. 2b). The statistical model $\delta^{13}C$ CO_2 data broadly agrees with *G. ruber* $\delta^{11}B$ CO_2 estimates in the Pliocene. However, it should be noted that our revised $\delta^{13}C_{C37}$ CO_2 agrees well with not only *T. sacculifer* $\delta^{11}B$ CO_2 (Dyez et al., 2018) but also T-inverse model derived CO_2 (van

245   de Wal et al., 2011; Berends et al., 2019) during the Pliocene in terms of both long-term trend and orbital-scale fluctuation.
Pliocene CO_2 estimates based on other independent proxies such as leaf stomata are below 360 ppm (Kürschner et al., 1996).
Also, the dynamic range of *G. ruber* $\delta^{11}B$ CO_2 (300-480 ppm) in the Pliocene is approximately twice as much as that of the
deep glacial-interglacial cycles (180-280 ppm) in the late Pleistocene (Siegenthaler et al., 2005; Lüthi et al., 2008), despite the
latter exhibiting smaller orbital-scale climate variations compared to that of the late Pleistocene. Furthermore, the fluctuation

250   range of the statistical model CO_2 in the Pliocene (200-620 ppm) is much larger than that of *G. ruber* $\delta^{11}B$ CO_2 (Stoll et al.,
2019) (Fig. 2b). Such a large fluctuation is difficult to explain given that G-IG climate fluctuation in Pliocene is much smaller
than that of the late Pleistocene.

3.7 Consideration of the discrepancy among the CO_2 proxies

A large offset of CO_2 estimates also exists between *G. ruber* and *T. sacculifer* $\delta^{11}B$ proxies throughout the Plio-Pleistocene

255   (Dyez et al., 2018). *T. sacculifer* $\delta^{11}B$ CO_2 records show relatively low values (well below 350 ppm) during the Pliocene
(Bartolri et al., 2011; Dyez et al., 2018), while many *G. ruber* $\delta^{11}B$ CO_2 values are above 350 ppm (Seki et al., 2010; Martínez-
Botí et al., 2015; de la Vega et al., 2020) (Fig. 5b). Potential causes for the discrepancy have been discussed in Dyez et al.
(2018) and de la Vega et al. (2020). They argued that biological effects such as long-term evolution of either foraminifera
species might alter the relationship between $\delta^{11}B$ and carbonate chemistry. On the other hand, de la Vega et al. (2020) argue

260   that the offset may be attributed to an analytical issue with *T. sacculifer* $\delta^{11}B$. However, the revised alkenone CO_2 records
agree well with *T. sacculifer* $\delta^{11}B$ CO_2 (Fig. 5b), suggesting alternation of *G. ruber* $\delta^{11}B$ CO_2 due to the biological effect.
Alternatively, another possible explanation for the high estimates of *G. ruber* $\delta^{11}B$ CO_2 is that those CO_2 records overestimate
variability ranges possibly due calibration for the conversion of *G. ruber* $\delta^{11}B$ into CO_2 concentration not being well-optimized.
It is worth noting that the *T. sacculifer* $\delta^{11}B$ CO_2 of Dyez et al. (2018) is re-estimated based on updated calibrations, with a

265   significant downward revision of Pliocene CO_2 compared to the original values (Bartoli et al., 2011) (Fig. 6). For conversion
of *G. ruber* $\delta^{11}B$ into CO_2, the culture and global core top calibration of Henehan et al. (2013) have been applied. However, it
should be noted that the number of the culture data, which is used to establish the calibration, is limited. Although *G. ruber*
$\delta^{11}B$ CO_2 in ODP 999 seems to well represent the CO_2 variability during the glacial-interglacial cycles documented in the
Antarctic ice core record (Foster et al., 2008; Chalk et al., 2017), a close look reveals that the variability range of *G. ruber* $\delta^{11}B$

270   CO_2 (150 to 340 ppm) is significantly larger than that of the ice-cores (180 to 280 ppm) (Fig. 2c). This suggests that *G.
ruber* $\delta^{11}B$ CO_2 overestimates the variability of CO_2 in the G-IG cycles. On the other hand, the dynamic range of *T. sacculifer*
$\delta^{11}B$ CO_2 (175-300 ppm) (Dyez et al., 2018), which shows relatively low CO_2 in the Pliocene, agrees well with ice core values
(180-280 ppm) (Fig. 2c) during the past 800 kyrs, supporting the reliability of CO_2 estimates. The variation range (150-350
ppm) of the statistical model $\delta^{13}C_{C37}$ CO_2 in the late Pleistocene also significantly exceeds that of ice core (180-280 ppm) (Fig.

275   2c), suggesting overcorrection of environmental factors. These considerations depict that the CO_2 records, which overestimate
CO_2 variation range during the Late Pleistocene G-IG cycles, show high CO_2 estimates in the Pliocene.

Further studies for developing the calibrations and constraints of environmental and physiological factors will be needed to generate robust CO_2 estimates. As for the alkenone $\delta^{13}C$ CO_2 proxy, these are ongoing efforts within the community (Zhang et al., 2020; Phelps et al., 2020; Badger, 2021) and include refinements to the alkenone CO_2 model (Zhang et al., 2020), culture

280 based constrains (Phelps et al., 2020) and consideration of the lower limits of the proxy due to CCMs (Badger, 2021). Here we highlight how relatively simple refinements for export production depth of alkenones (based on $U^{K'}_{37}$ temperature) and using regional $[PO_4^{3-}]$ depth profiles can lead to major reconciliation of CO_2 estimates with other lines of evidence.

4 Conclusion

In this study, previously reported $\delta^{13}C_{C37}$ based CO_2 records from the Plio-Pleistocene were reexamined to better constrain

285 CO_2 evolution. We refined the conventional approach, which assumes constant physiological factors and a carbon diffusive model over the time by including considerations of regional differences in physical oceanographic factors, specifically the mixed layer depth, production season and air-ocean disequilibrium of CO_2 for each site (Fig. 4). This simple approach refines estimates of CO_2 significantly, reducing large offsets previously observed in the reported $\delta^{13}C_{C37}$ CO_2 records from different oceanographic settings. However, some of our data still do not obtain sufficiently low glacial CO_2 values during the Pleistocene

290 (Fig. 4d). This suggests varying physiological factors associated with G-IG cycles or upregulation of carbon concentration mechanisms in glacial low CO_2 conditions at some sites. Nevertheless, this study shows that better constraints on past environmental variables can be obtained using literature data and this this approach can improve $\delta^{13}C_{C37}$ CO_2 estimates. Our revised $\delta^{13}C_{C37}$ CO_2 datasets are consistent well with the previously reported CO_2 estimates in the early to mid Pleistocene (Da et al., 2019; Dyez et al., 2018; Cui et al., 2020) with CO_2 levels below 300 ppm. On the other hand, the revised $\delta^{13}C_{C37}$ CO_2

295 CO_2 levels in the Pliocene are lower than 350 ppm. Our low CO_2 values in the Pliocene are consistent with other CO_2 estimates such as a T-inverse model (van de Wal et al., 2011; Berends et al., 2019), *T. sacculifer* $\delta^{11}B$ (Bartoli et al., 2011; Dyez et al., 2018) and leaf stomata (Kürschner et al., 1996) based CO_2 reconstructions (Fig. 5b), albeit the upper end of the Pliocene CO_2 are lower than that of *G. ruber* $\delta^{11}B$ (Seki et al., 2010; Martínez-Botí et al., 2015; de la Vega et al., 2020) and statistical model $\delta^{13}C_{C37}$ (Stoll et al., 2019) CO_2 estimates. Further efforts are needed to constrain the dynamic range of CO_2 for time periods

300 pre-dating the ice core records. It is particularly important to generate continuous, high temporal resolution CO_2 records which overlap and match the Antarctic ice-core CO_2 records.

Author contributions

O.S. and J.B. analysed the paleoclimatic data and wrote the manuscript.

Competing interests

305   The authors declare that they have no conflicts of interest.

Acknowledgments

Samples used in this research were provided by the Ocean Drilling Program (ODP). This research is supported by the Japan
Society of Promotion of Science (No. 26287129 and 17H06318) grant awarded to OS funded by the Ministry of Education,
Culture, Sports, Science and Technology, Japan. JB thanks the Japan Society of Promotion of Science for a BRIDGE short-
310   term Research Fellowship.

References

Anagnostou, E., John, E. H., Edgar, K. M., Foster, G. L., Ridgwell, A., Inglis, G. N., Pancost, R. D., Lunt, D. J. and Pearson,
   P. N.: Changing atmospheric CO_2 concentration was the primary driver of early Cenozoic climate, Nature, 533, 380–384,
   2016.

315   Anagnostou, E., John, E. H., Babila, T. L., Sexton, P. F., Ridgwell, A., Lunt, D. J., Pearson, P. N., Chalk, T. B., Pancost, R. D.
   and Foster, G. L.: Proxy evidence for state-dependence of climate sensitivity in the Eocene greenhouse, Nat. Cummun. 11,
   4436, 2020.

Badger, M. P. S, Schmidt, D., Mackensen, A. and Pancost, R.: High-resolution alkenone palaeobarometry indicates relatively
   stable pCO_2 during the Pliocene (3.3–2.8 Ma), Phil. Trans. R. Soc. A, 371, doi: 10.1098/rsta.2013.0094, 2013.

320   Badger, M.P.S. Chalk, T. B., Foster, G. L., Bown, P. R., Gibbs, S. J., Sexton, P. F., Schmidt, D. N., Pälike, H., Mackensen,
   A. and Pancost, R. D.: Insensitivity of alkenone carbon isotopes to atmospheric CO_2 at low to moderate CO_2 levels, Clim.
   Past, 15, 539-554, 2019.

Badger M. P. S.: Alkenone isotopes show evidence of active carbon concentrating mechanisms in coccolithophores as aqueous
   carbon dioxide concentrations fall below 7 μmol L^{-1}, Biogeosci., 18, 1149-1160, 2021.

325   Bartoli, G., Hönisch, B. and Zeebe, R. E.: Atmospheric CO_2 decline during the Pliocene intensification of Northern Hemisphere
   glaciation, Paleoceanogr., 26, 2010PA002055, 2011.

Beerling, D. J. and Royer, D. L.: Convergent Cenozoic CO_2 history. Nat. Geosci., 4, 418-420, 2011.

Benthien, A., Anderson, N., Schulte, S., Müller, P., Schneider, R. R. and Wefer, G.: The carbon isotopic record of the $C_{37:2}$
   alkenone in the South Atlantic: Last Glacial Maximum (LGM) vs. Holocene, Palaeogeogr. Palaeoclimatol. Palaeoecol., 221,
330   123– 140, 2005.

Berends, C. J., de Boer, B., Dolan, A. M., Hill, D. J. and van de Wal, R. S. W.: Modelling ice sheet evolution and atmospheric
   CO2 during the Late Pliocene, Clim. Past, 15, 1603-1619, doi.org/10.5194/cp-15-1603-2019, 2019.

Bidigare, R.R., Fluegge, A., Freeman, K. H., Hanson, K. L., Hayes, J. M., Hollander, D., Jasper, J. P., King, L. L., Laws, E. A., Milder, J., Millero, F. J., Pancost, R., Popp, B. N., Steinberg, P. A. and Wakeham, S. G.: Consistent fractionation of ^{13}C in nature and in the laboratory: Growth-rate effect in some haptophyte algae, Global Biogeochem. Cy., 11, 279-292, 1997.

Bidigare, R.R., Fluegge, A., Freeman, K. H., Hanson, K. L., Hayes, J. M., Hollander, D., Jasper, J. P., King, L. L., Laws, E. A., Milder, J., Millero, F. J., Pancost, R., Popp, B. N., Steinberg, P. A. and Wakeham, S. G.: Correction to "Consistent fractionation of ^{13}C in nature and in the laboratory: Growth-rate effect in some haptophyte algae", Global Biogeochem. Cy., 13, 251-252, 1999.

Bolton, C. and Stoll, H. M.: Late Miocene threshold response of marine algae to carbon dioxide limitation, Nature, 500, 558-562, 2013.

Bolton, C., Hernández-Sánchez, M.-T., Fuertes, M.-Á., González-Lemos, S., Abrevaya, L., Mendez-Vicente, A., Flores, J.-A., Probert, I., Giosan, L., Johnson, J. and Stoll, H. M.: Decrease in coccolithophore calcification and CO_2 since the middle Miocene, Nat. Commun., 7, 10.1038/ncomms10284, 2015.

Brierley, C. M. and Fedorov, A. V.: Relative importance of meridional and zonal sea surface temperature gradients for the onset of the ice ages and Pliocene-Pleistocene climate evolution, Paleoceanogr. Paleoclimatol., 25, PA2214, doi:10.1029/2009PA001809, 2010.

Chalk, T. B., Hain, M. P., Foster, G. L., Rohling, E.J., Sexton, P. F., Badger, M. P. S., Cherry, S. G., Hasenfratz, A. P., Haug, G. H., Jaccard, S. L., Martínez-García, A., Pälike, H., Pancost, R. D. and Wilson, P. A.: Causes of ice age intensification across the mid-Pleistocene transition, P. Natl. Acad. Sci. USA, 114, 13114–13119, 2017.

Conte, M. H., Sicre, M.-A. Rühlemann, C. Weber, J. C., Schulte, S., Schulz-Bull, D. and Blanz, T.: Global temperature calibration of the alkenone unsaturation index ($U^{K'}_{37}$) in surface waters and comparison with surface sediments, Geochem. Geophys. Geosyst. 7, 2005GC001054, 2006.

Cui, Y., Schubert, B. A. and Jahren, A. H.: A 23 m.y. record of low atmospheric CO_2, Geology, 48, 888-892, 2020.

Da, J., Zhang, Y. G., Li, G., Meng, X., Ji, J.: Low CO_2 levels of the entire Pleistocene Epoch, Nat. Commun., 10, 4342, doi .org/10.1038/s41467-019-12357-5, 2019.

de la Vega, E., Chalk, T. B., Wilson, P. A., Bysani, R. P. and Foster, G. L.: Atmospheric CO_2 during the Mid-Piacenzian Warm Period and the M2 glaciation, Sci. Rep., 10, 11002, 2020.

Dyez, K. A., Hönisch, B., Schmidt, G. A.: Early Pleistocene Obliquity-Scale pCO_2 variability at ~1.5 million years ago, Paleoceanogr. Paleoclimatol., 33, 1270-1291, doi.org/10/1029/2018PA003349, 2018.

Eek, M. E., Whiticar, M. J., Bishop, J. K. and Wong, C. S.: Influence of nutrients on carbon isotope fractionation by natural populations of Prymnesiophyte algae in NE Pacific, Deep-Sea Res. II, 46, 2863-2876, 1999.

Foster, G. L.: Seawater pH, pCO_2 and $[CO_3^{2-}]$ variations in the Caribbean Sea over the last 130 kyr: A boron isotope and B/Ca study of planktic foraminifera, Earth Planet. Sci. Lett., 271, 254–266, 2008.

365   Greenop, R., Foster, G. L., Wilson, P. A. and Lear, C. H.: Middle Miocene climate instability associated with high-amplitude
        CO2 variability, Paleoceanogr., 29, 845-843, 2014.

        Henderiks, J. and Pagani, M.: Refining ancient carbon dioxide estimates: Significance of coccolithophore cell size for
        alkenone-based pCO$_2$ records, Paleoceanogr., 22, PA3202, doi:10.1029/2006PA001399, 2007.

        Henehan, M. J., Rae, J. W. B., Foster, G. L., Erez, J., Prentice, K. C., Kucera, M., Bostock, H. C., Martínez-Botí, M. A., Milton,
370   A., Wilson, P. A., Marshall, B. J. and Elliott, T.: Calibration of the boron isotope proxy in the planktonic foraminifera
        Globigerinoides ruber for use in palaeo-CO$_2$ reconstruction, Earth Planet. Sci. Lett., 364, 111–122,
        doi.org/10.1016/j.epsl.2012.12.029, 2013.

        Higgins, J. A., Kurbatov, A. V., Spaulding, N. E., Brook, E., Introne, D. S., Chimiak, L. M., Yan, Y., Mayewski, P. A., and
        Bender, M. L.: Atmospheric composition 1 million years ago from blue ice in the Allan Hills, Antarctica, P. Natl. Acad. Sci.
375   USA, 112, 6887-6891, 2015.

        Hönisch, B., Hemming, N. G., Siddall, M., McManus, J. F.: Atmospheric carbon dioxide concentration across the Mid-
        Pleistocene Transition, Science, 324, 1551-1554, 10.1126/science.1171477, 2009.

        Jasper, J. P., Hayes, J. M., Mix, A. C. and Prahl, F.G.: Photosynthetic fractionation of ^{13}C and concentrations of dissolved CO$_2$
        in the central equatorial Pacific during the last 255,000 years, Paleoceanogr., 9, 781-798, 1994.

380   Kameo, K. and Sato, T.: Biogeography of Neogene calcareous nannofossils in the Caribbean and the eastern equatorial Pacific
        – floral response to the emergence of the Isthmus Panama, Mar. Micropaleontol., 39, 201-218, 2000.

        Kameo, C. and Bralower, T.: Neogene calcareous nannofossil biostratigraphy of sites 998, 999, and 1000, Caribbean Sea, P.
        ODP Sci. Res., 165, 3-17, 2000.

        Kürschner, W. M., van de Burgh, J., Visscher, H. and Dilcher, D. L.: Oak leaves as biosensors of late Neogene and early
385   Pleistocene paleoatmospheric CO$_2$ concentrations, Mar. Micropaleontol., 27, 299-312, 1996.

        Kürschner W. M., Kvaček, Z. and Dilcher, D. L.: The impact of Miocene atmospheric carbon dioxide fluctuations on climate
        and the evolution of terrestrial ecosystems, P. Natl. Acad. Sci. USA, 105, 449-453, 2008.

        Laws, A., Popp, B. N. Bidigare, R. R., Riebesell, U. Burkhardt, S. and Wakeham, S. G.: Controls on the molecular distribution
        and carbon isotopic composition of alkenones in certain haptophyte algae, Geochem. Geophys. Geosyst., 2, 2000GC000057,
390   2001.

        Lisiecki, L. E. and Raymo, M. E. A.: Pliocene-Pleistocene stack of 57 globally distributed benthic δ^{18}O records, Paleoceanogr.,
        20, PA1003, doi:10.1029/2004PA001071, 2005.

        Locarnini, R. A., Mishonov, A. V., Antonov, J.-I. and Boyer, T.-P.: World Ocean Atlas 2009, Vol. 1: Temperature, S. Levitus,
        Ed. NOAA Atlas NESDIS 68, U.S. Government Printing Office, Washington, D.C., 184 pp, 2009.

395   Lüthi, D., Floch, M. L., Bereiter, B., Blunier, T., Barnola, J.-M., Siegenthaler, U., Raynaud, D., Jouzel, J., Fischer, H.,
        Kawamura, K. and Stocker, T. F.: High-resolution carbon dioxide concentration record 650,000–800,000 years before
        present, Nature, 453, 379–382, 2008.

Martínez-Botí, M. A., Foster, G. L., Chalk, T. B., Rohling, E. J., Sexton, P. F., Lunt, D. J., Pancost, R. D., Badger, M. P. S. and Schmidt, D. N.: Plio–Pleistocene climate sensitivity evaluated using high-resolution CO_2 records, Nature, 518, 49-54, 2015.

Mejia, L. M., Méndez-Vicente, A., Abrevaya, L., Lawrence, K. T., Ladlow, C., Bolton, C., Cacho, I. and Stoll, H.: A diatom record of CO_2 decline since the late Miocene, Earth Planet. Sci. Lett., 479, 18-33, 2017.

Mix, A. C. et al.: Chapter 12, Site 1241. Proc. ODP Init. Repts., 202, doi:10.2973/odp.proc.ir.202.112.2003, 2003.

Mook, W. G., Bommerson, J. C. and Staverman, W. H.: Carbon isotope fractionation between dissolved bicarbonate and gaseous carbon dioxide, Earth Planet. Sci. Lett. 22, 169-176, 1974.

Pagani, M. et al., 2002. Comparison of water column [CO_{2aq}] with sedimentary alkenone-based estimates: A test of the alkenone-CO_2 proxy. Paleoceanography 17, doi:10.1029/2002PA000756.

Pagani, M. et al., 2005. Marked decline in atmospheric carbon dioxide concentrations during the Paleogene. Science 309, 600-603.

Pagani, M. et al., 2010. High Earth-system climate sensitivity determined from Pliocene carbon dioxide concentrations. Nat. Geosci. 3, 27-30.

Pagani, M., Huber, M., Liu, Z., Bohaty, S. M., Henderiks, J., Sijp, W., Krishnan, S. and DeConto, R. M.: The role of carbon dioxide during the onset of Antarctic Glaciation, Science, 334, 1261-1264, 2005.

Pearson, P. N., Foster, G. L. and Wade, B. S.: Atmospheric carbon dioxide through the Eocene-Oligocene climate transition, Nature, 461, 1110–1113, 2009.

Phelps, A. R. et al.: Harmonizing Miocene alkenone- and boron-based carbonate chemistry reconstructions, AGU Fall Meeting 2020, PP007-06, 2020.

Plancq, J., Grossi, V., Henderiks, J., Simon, L. and Mattioli, E.: Alkenone producers during late Oligocene-early Miocene revisited, Paleoceanogr., 27, 2011PA002164, 2012.

Popp, B. N., Laws, E. A. Bidigare, R. R., Dore, J. E., Hanson, K. L. and Wakeham, S. G.: Effect of phytoplankton cell geometory on carbon isotopic fractionation, Geochim. Cosmochim. Acta, 62, 69-77, 1998.

Popp, B. N., Hanson, K. L., Dore, J. E., Bidigare, R. R., Laws, E. A. and Wakeham, S. G.: Controls on the carbon isotopic composition of phytoplankton: Paleoceanographic perspec-tives, in Reconstructing Ocean History: A Window into the Future, F. Abrantes, A. Mix, Eds. (Plenum, New York), pp. 381–398, 1999.

Raitzsch, M., Bijma, J., Bickert, T., Schulz, M., Holbourn, A. and Kučera1, M.: Atmospheric carbon dioxide variations across the middle Miocene climate transition, Clim. Past, 17, 703-719, 2021.

Raven, J. A., Ciordano, M., Beardall, J. and Maberly, S. C.: Algal and aquatic plant carbon concentrating mechanisms in relation to environmental change, Photosynth. Res., 109, 281–296, 2011.

Reinfelder, J. R.: Carbon concentrating mechanisms in eukaryotic marine phytoplankton, Annu. Rev. Mar. Sci., 3, 291–315, 2011.

Romanek, C. S., Grossman, E. L. and Morse, J. W.: Carbon isotopic fractionation in synthetic aragonite and calcite: Effects of temperature and precipitation rate. Geochim. Cosmochim. Acta, 56, 419-430, 1992.

Seki, O., Foster, G. L., Schmidt, D. N., Mackensen, A., Kawamura, K. and Pancost, R. D.: Alkenone and boron-based Pliocene pCO_2 records, Earth Planet. Sci. Lett., 292, 201–211, 2010.

435 Siegenthaler, U., Monnin, E., Kawamura, K., Spahni, R., Schwander, J. and Stauffer, B.: Supporting evidence from the EPICA Dronning Maud Land ice core for atmospheric CO_2 changes during the past millennium. Tellus Ser. B, 57, 51–57, 2005.

Sonzogni, C., Bard, E., Rostek, F., Lafont, R., Rosell-Mele, A. and Eglinton, G.: Core-top calibration of the alkenone index vs sea surface temperature in the Indian Ocean, Deep-Sea Res. II, 44, 1445–1460, 1997.

Spero, H. J., Bijma, J., Lea, D. W. and Bemis, B. E.: Effect of sea water carbonate concentration on foraminiferal carbon and 440 oxygen isotopes, Nature, 390, 497-500, 1997.

Stoll, H. M., Guitian, J., Hernandez-Almeida, I., Mejia, L. M., Phelps, S., Polissar, P., Zhang, H. and Ziveri, P.: Upregulation of phytoplankton carbon concentrating mechanisms during low CO_2 glacial periods and implications for the phytoplankton pCO_2 proxy, Quat. Sci. Rev., 208, 1-20, 2019.

Takahashi, T. et al.: Climatological mean and decadal change in surface ocean pCO_2 and net sea-air CO_2 flux over the global 445 oceans, Deep-Sea Res. II, 56, 554-577, 2009.

Voosen, P.: 2.7-million-year-odl ice opens window on past, Science, 357, 630-631, 2017.

Weiss, R. F.: Carbon dioxide in water and seawater: the solubility of a non-ideal gas, Mar. Chem., 2, 203-215, 1974.

Yan, Y., Bender, M. L., Brook, E. J., Clifford, H. M., Kemeny, P. C., Kurbatov, A. V., Mackay, S., Mayewski, P. A., Ng, J., Severinghaus, J. P. and Higgins, J. A.: Two-million-year-old snapshots of atmospheric gases from Antarctic ice, Nature, 450 574, 663-666, 2019.

Zhang, Y. G., Pagani, M., Liu, Z., Bohaty, S. M. and DeConto, R.: A 40-million-year history of atmospheric CO_2, Phil. Trans. R. Soc. A, 371, 10.1098/rsta.2013.0096, 2013.

Zhang, Y. G., Pearson, A., Benthien, A., Dong, L., Huybers, P., Liu, X. and Pagani, M.: Refining the alkenone-pCO_2 method I: Lesson from the Quaternary glacial cycles, Geochim. Cosmochim. Acta, 260, 177-191, 2019.

455 Zhang, Y.G., Henderiks, J., Liu, X.: Refining the alkenone-pCO_2 method II: Towards resolving the physiological parameter 'b', Geochim. Cosmochim. Acta, 281, 118-134, 2020.

Table 1. Location of ODP samples, surface mixed layer depth (SML), sea-air ΔCO_2 in surface water, sea surface salinity (SSS) and regression applied to calculate b-term.

Site	Modern location	SML (m)	$[PO_4^{3-}]$ at SML (uM/L)	ΔCO_2 (μatm)	SSS (psu)	b-term regression	SST calibration
ODP 806	0.5N, 159.5E	0-50	0.14-0.18	30	35	EP	Sonzogni et al. (1997)
ODP 925	4.5N, 43.5W	0-30	0.16-0.08	22	35	Global	Sonzogni et al. (1997)
ODP 982	57.5N, 16W	0-30	0.52-0.55	-32	35	Global	Conte et al. (2006)
ODP 999	12.5N, 78.4W	0-30	0.05-0.08	17	36	BA	Sonzogni et al. (1997)
ODP 1208	36.5N, 158.5E	0-20	0.22-0.28	-38	35	Global	Conte et al. (2006)
ODP 1241	5.5N, 86.5W	0-10	0.32-0.38	14	32	EP	Sonzogni et al. (1997)

BA = Bermuda Atlantic. EP = Equatorial Pacific.

460
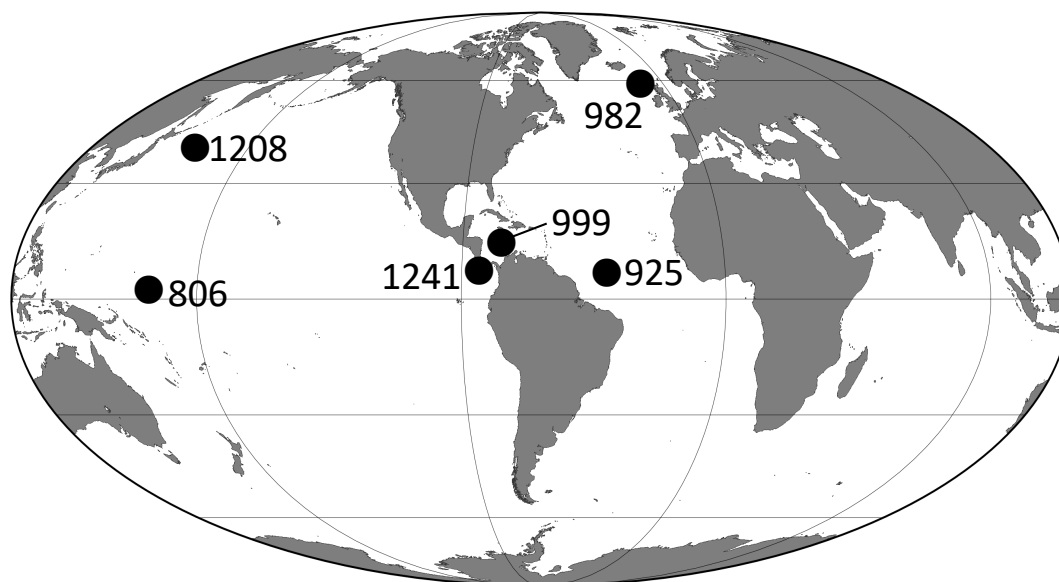
Figure 1: Locations of ODP sediment core sites used for CO₂ reconstructions.
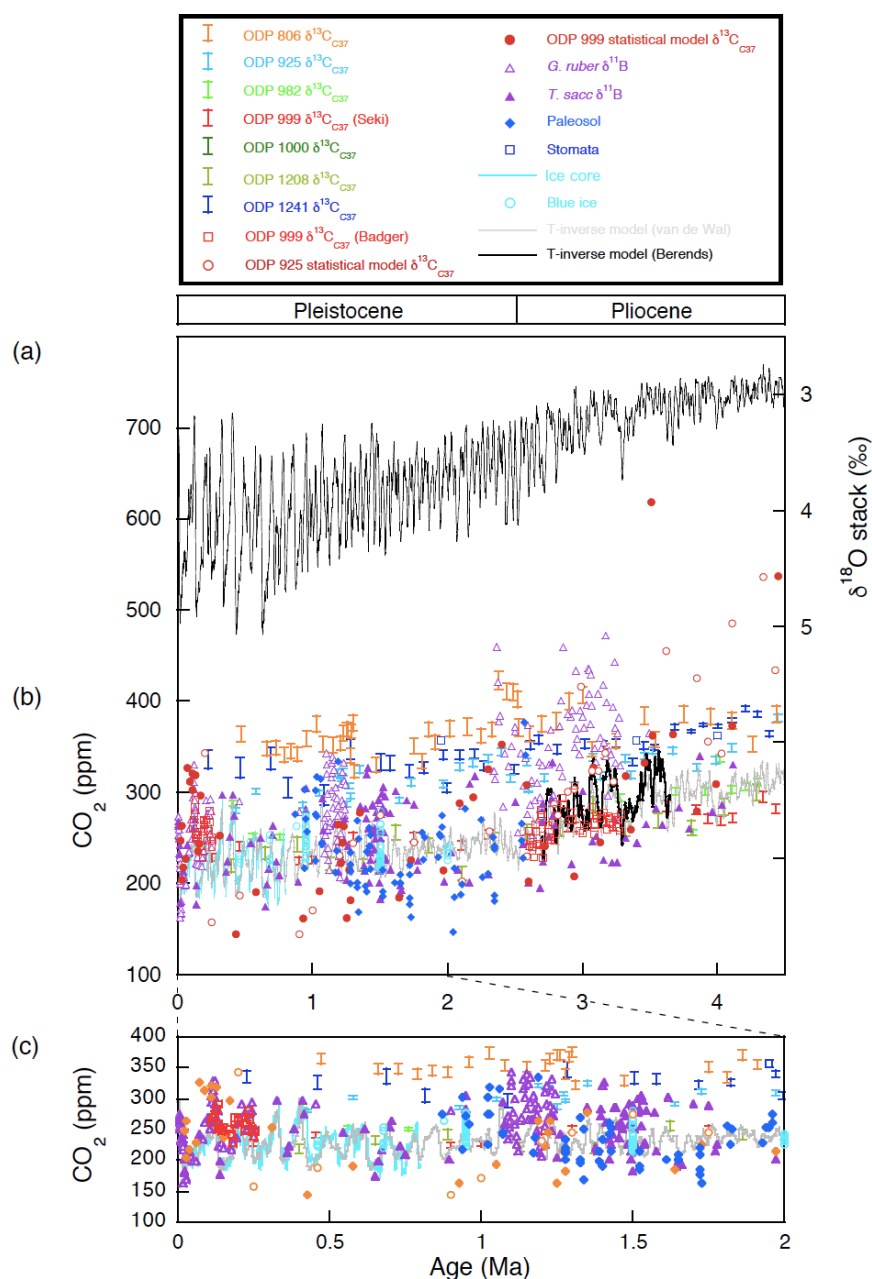
Figure 2: (a) Benthic $\delta^{18}O$ stack (Lisiecki and Raymo, 2005), $\delta^{13}C_{C37}$, $\delta^{11}B$ and paelosol CO_2 records over the past (b) 5 Myrs and (c) 2 Myrs together with Antarctic ice core and blue ice CO_2. Open purple triangle: *G. ruber* $\delta^{11}B$ CO_2 records in ODP 999 (Foster et al ,2008; Seki et al., 2010; Martínez-Botí et al., 2015; Chalk et al. ,2017; de la Vega et al., 2020). Solid purple triangle: *T. sacculifer* $\delta^{11}B$ CO_2 records in ODP 668 and 999 (Hönisch et al., 2009; Bartoli et al., 2011; Dyez et al., 2018). Light blue line: ice core CO_2 (Siegenthaler et al., 2005; Lüthi et al., 2008). Open light blue circle: blue ice CO_2 (Higgins et al., 2015; Yan et al., 2019). Bar: $\delta^{13}C_{C37}$

470 **CO₂ records in ODP 806 (orange), ODP 925 (light blue), ODP 982 (light green), ODP 999 (red), ODP 1208 (dark green) and ODP 1241 (blue) (Pagani et al., 2010; Seki et al., 2010). Error bars represent a range calculated assuming production depths (surface mixed layer). Open red circle: δ¹³C_C37 CO₂ records in ODP 999 (Badger et al., 2013, 2019). Open and solid brown circles: statistical model δ¹³C_C37 CO₂ records in ODP 925 and 999, respectively (Stoll et al., 2019). Open blue square: Stomata CO₂ records (Kürschner et al., 1996). Solid blue diamond: paleosol CO₂ (Da et al., 2019). Grey and black lines: T-inverse model CO₂ (van de Wal et al., 2011;**
475 **Berends et al., 2019).**
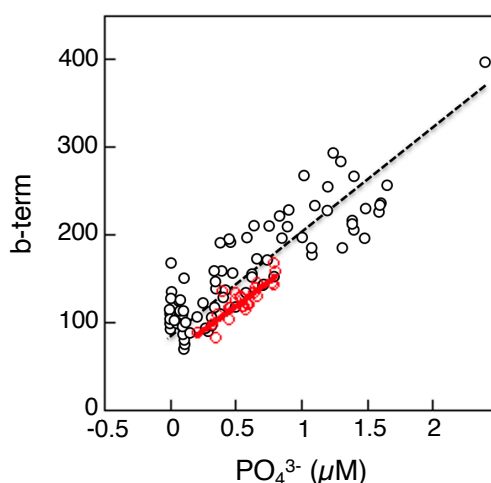
Figure 3: Scatter plot of phosphate concentration and b-term (Bidigare et al., 1997, 1999; Eek et al., 1999; Laws et al., 2000). Open red circles represent Equatorial Pacific data including Equatorial Pacific (fall and spring) and Iron Ex (Bidigare et al., 1997) while
480 **open black circles are data from other regions. Red line: Equatorial Pacific (EP) regression. Black dashed line: the global regression (Pagani et al., 2005).**
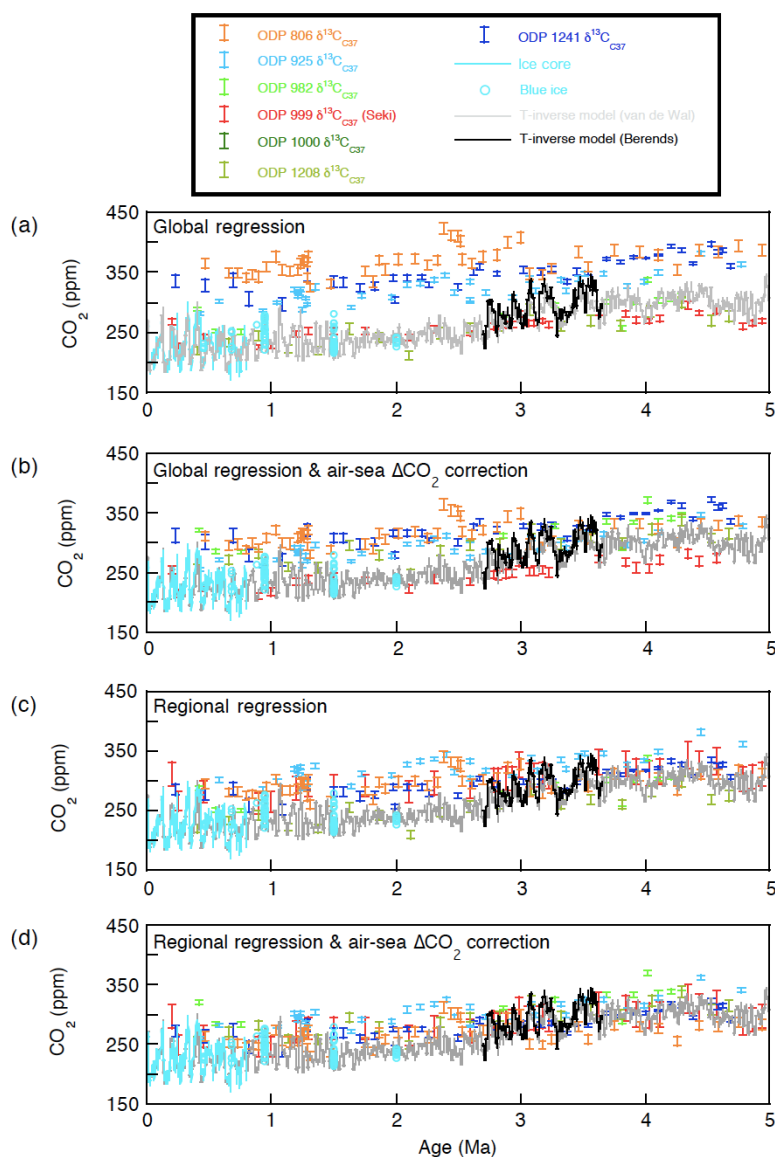
Figure 4: **δ¹³C$_{C37}$ CO$_2$ records over the past 5 Myrs together with ice core CO$_2$ (light blue line) (Siegenthaler et al., 2005; Lüthi et al.,**
2008), blue ice CO$_2$ (open light blue circle) (Higgins et al., 2015; Yan et al., 2019) and T-inverse model derived CO$_2$ (grey and black
lines) (van de Wal et al., 2011; Berends et al., 2019). (a) CO$_2$ records based on the global regression (original data are from Pagani
et al. (2005) and Seki et al. (2010). (b) CO$_2$ records based on the global regression with accounting for air-sea ΔCO$_2$. (c) CO$_2$ records
based on the regional regressions. (d) CO$_2$ records based on the regional regressions records of (b) but also after correction of air-
sea ΔCO$_2$. Bar: δ¹³C$_{C37}$ CO$_2$ records in ODP 806 (orange), ODP 925 (light blue), ODP 982 (light green), ODP 999 (red), ODP 1208
(dark green) and ODP 1241 (blue) (Pagani et al., 2010; Seki et al., 2010).
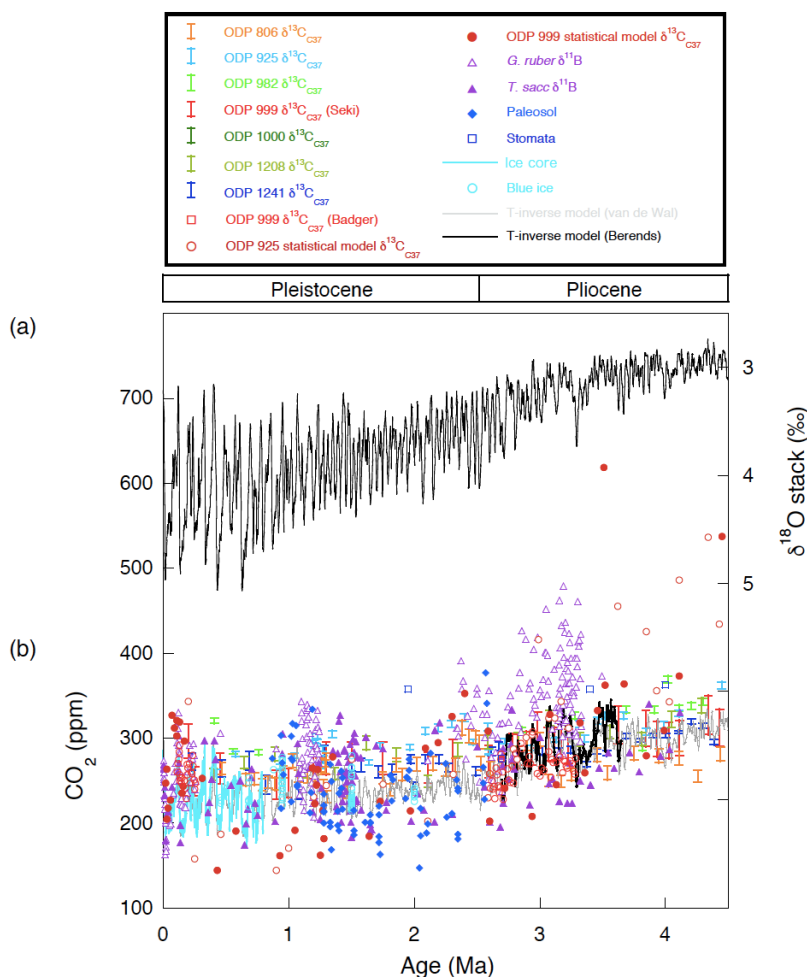
Figure 5: (a) Benthic δ¹⁸O stack (black line) (Lisiecki and Raymo, 2005) and (b) Corrected δ¹³C$_{C37}$, statistical model δ¹³C$_{C37}$, δ¹¹B and paleosol CO₂ records over the past 5 Myrs together with ice core CO₂ (light blue line) (Siegenthaler et al., 2005; Lüthi et al.,
495 **2008), blue ice CO₂ (open light blue circle) (Higgins et al., 2015; Yan et al., 2019) and T-inverse model derived CO₂ (grey and black lines) (van de Wal et al., 2011; Berends et al., 2019). Open blue triangle: *G. ruber* δ¹¹B CO₂ records in ODP 999 (Foster et al ,2008; Seki et al., 2010; Martínez-Botí et al., 2015; Chalk et al. ,2017; de la Vega et al., 2020). Solid purple triangle: *T. sacculifer* δ¹¹B CO₂ records in ODP 668 and 999 (Hönisch et al., 2009; Bartoli et al., 2011; Dyez et al., 2018). Open light blue circle: blue ice CO₂ (Higgins et al., 2015; Yan et al., 2019). Bar: δ¹³C$_{C37}$ CO₂ records in ODP 806 (orange), ODP 925 (light blue), ODP 982 (light green), ODP 999**
500 **(red), ODP 1208 (dark green) and ODP 1241 (blue) (Pagani et al., 2010; Seki et al., 2010). Open red circle: δ¹³C$_{C37}$ CO₂ records in ODP 999 (Badger et al., 2013, 2019). Open and solid brown circles: statistical model δ¹³C$_{C37}$ CO₂ records in ODP 925 and 999, respectively (Stoll et al., 2019). Open blue square: Stomata CO₂ records (Kürschner et al., 1996). Solid blue diamond: paleosol CO₂ (Da et al., 2019).**
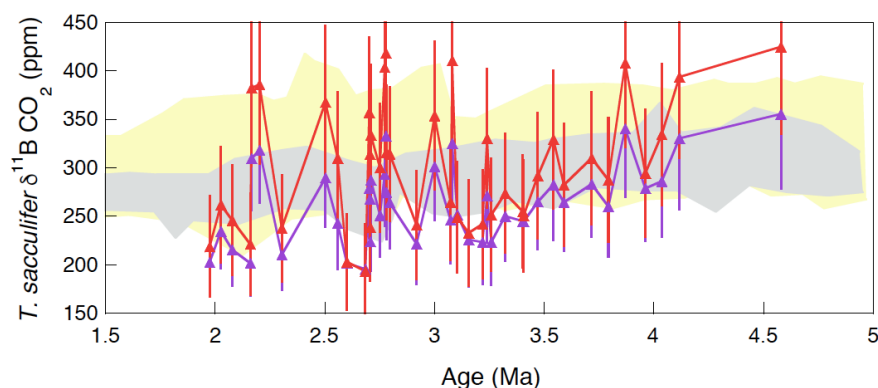
505

Figure 6: Original (red triangle; Bartoli et al., 2011) and revised (purple triangle; Dyez et al., 2018) *T. sacculifer* δ^{11}B CO$_2$ **records from the Pliocene to early Pleistocene. Yellow and grey areas represent ranges of reported (Pagani et al., 2010; Seki et al., 2010; Badger et al., 2013, 2019) and corrected (this study)** δ^{13}C$_{C37}$ CO$_2$, **respectively.**